Reduction of Aerodynamic Augmented States in Active Flutter Suppression Systems

E. Nissim*
NASA Ames Research Center, Moffett Field, California 94035

A method is proposed by which an aeroservoelastic problem is brought to a state-space form with a minimum number of augmented aerodynamic terms. The examples treated in this work relate to NASA's Drone for Aerodynamic and Structural Testing, Aerodynamic Research Wing 1, and to the YF-17 fighter model. It is shown that, in all cases considered, the method yields a very good accuracy regarding the flutter parameters and the dynamic behavior of the systems, using only two augmented aerodynamic states. The method should prove useful in the design of lower order control laws based on optimal control theory.

Nomenclature

$A_{l_{ij}}$ = element i,j of aerodynamic matrix $[A_l]$
b = reference semichord length, or semichord length at the spanwise section where accelerometer is located
c = wing chord, $=2b$
h = displacement of sensor, positive down
k = reduced frequency, $=\omega b/V$
M = Mach number
n = number of modes
n_a = number of augmented aerodynamic states
n_{col} = number of columns in the equations of motion
n_i = number of important flutter modes
n_L = number of lag terms
n_{L_j} = number of lag terms associated with the jth column of the aerodynamic matrix
n_r = number of rows in the equation of motion
s = Laplace variable
Q_D = fluid dynamic pressure
V = fluid velocity
β = leading-edge control deflection
β_l = the lth lag term in the Padé representation
$\beta_{l_{ij}}$ = value for β_l for matrix element i,j
δ = trailing-edge control deflection
δ_c = command trailing-edge control deflection
ω = frequency of oscillation

Matrix Notation

$[A]$ = tabulated matrix of aerodynamic coefficients; also plant state matrix
$[\bar{A}]$ = matrix of aerodynamic coefficients expressed in Padé form
$[B_l]$ = matrix of aerodynamic coefficients, also control input matrix [see Eq. (15)]
$[D]$ = the plant equation in state-space form
$[K]$ = stiffness matrix
$[M]$ = mass matrix
$\{q\}$ = response vector
$\{x_\beta\}$ = vector of augmented aerodynamic states
$\{x_{\beta j}\}$ = vector of aerodynamic states, defined in Eq. (5)

Subscripts

ac = associated with actuator
c = associated with control surfaces
F = associated with flutter
G = associated with gust input
outb = associated with DAST-ARW1 outboard accelerometer
s = associated with structural modes
s,LE = associated with sensor driving the leading-edge control
s,TE = associated with sensor driving the trailing-edge control

I. Introduction

THE equations of motion of a flexible aircraft contain unsteady aerodynamic terms that can only be approximated to assume algebraic form. The most common form of approximation involves rational functions, often referred to as Padé functions. However, although the Padé representation leads to linear time-invariant equations of motion in state-space form, it also gives rise to an increased number of states. The number of states associated with the Padé representation of the aerodynamic forces is often referred to as to the number of aerodynamic augmented states. A realistic aeroservoelastic case, for example, with 10 structural modes, may lead to equations of motion with around 60–70 states, out of which there may be as many as 40 aerodynamic augmented states. This aerodynamic augmentation of the order of the plant leads to serious disadvantages since many optimal control methods yield optimal feedback control laws of the same high order as the plant (since an estimator is always required in aeroelastic problems). These high-order control laws are often too complex to implement on a flight computer.

One obvious way of reducing the order of the resulting optimal control law is to consider, in the equations of motion, as few modes as possible. It is well known that the open-loop flutter instability is caused invariably by the mutual interaction of around two to three modes, and, therefore, one might be tempted to consider only those modes in the design process of active control laws. However, a typical control law normally feeds back the acceleration sensed at a specific location on the wing, and this acceleration is composed of many modes, not only of those modes responsible for flutter. Hence, if the modes that are not responsible for flutter are ignored in the closed-loop synthesis of the control law, the actual feedback might lead to degraded performance of the closed-loop system, or it might lead to the destabilization of the other

Received Oct. 11, 1989; revision received May 1, 1990; accepted for publication May 7, 1990.

*NRC Research Associate, Dryden Flight Research Center; on leave from Technion—Israel Institute of Technology, Department of Aerospace Engineering. Member AIAA.

modes that, as stated earlier, are otherwise stable (in the open-loop case). One may ignore only those modes with sufficiently high frequency, based on the assumption that their contributions to the sensed acceleration is negligible, or that the control deflections at those high frequencies are negligible (due to the attenuation caused by the actuator and the control law). Therefore, one is forced to consider a relatively large number of modes in the synthesis process, with the eventual result of high-order optimal control laws. As a result, many special methods have been proposed to reduce the order of the synthesized control laws. These methods can be divided into two main groups. The first group deals with methods that attempt to yield low-order control laws, using large-order plants.[1-4] These methods are inherently approximate and have deficiencies that will not be discussed herein. The second group of methods[5-8] concentrates on the Padé representation of the aerodynamic forces and attempts to obtain a good aerodynamic representation with a minimum number of resulting aerodynamic augmented states. The present work falls within this latter group of methods. It will, therefore, be the prime purpose of this work to propose a way of reducing the number of the augmented aerodynamic states to a minimum, while maintaining a good physical representation of the aeroservoelastic problem.

II. Proposed Approach

In all the Padé methods mentioned earlier, the different parameters in the Padé representation are determined either by minimizing the overall least-square errors between the tabulated values of $A(ik)$ and those given by the assumed Padé representation, or by minimizing these errors for each of the aerodynamic terms separately. Constraints may be imposed during the solution so as to match the tabulated and the fitted aerodynamic coefficients at various chosen values of reduced frequencies. Weighting may be applied to give more weight to the errors of some desired aerodynamic coefficients over a specified range of reduced frequencies. However, in all cases, with the exception of one (which will be mentioned in the following), the quality of the Padé approximation obtained and the reasoning for any weighting introduced is essentially numerical, aiming primarily at normalizing each coefficient and reducing the overall normalized error to a minimum (see Ref. 7, for example). No reference is made in these methods to the other terms in the equations of motion and to the importance of the relative values between the different aerodynamic terms and their inertia and stiffness counterparts. From a dynamic point of view, it is clear that not all aerodynamic terms are equally important. One can, for example, tolerate larger errors in the aerodynamic terms associated with the high-frequency modes (since the structural terms are large relative to the aerodynamic terms) or with the modes that are unimportant for flutter (since the aerodynamic lag terms are less important), with little effect on the dynamics of the system. Hence, physical reasoning is also essential in attempting to reduce the number of augmented aerodynamic states to a minimum. The only work that applies physical weighting to the least-square problem, based on dynamic consideration, is that by Karpel.[9] Karpel uses the minimum state approach and assigns different weights to the different terms, at the different k values, with more weight given to parameters where the open-loop modal eigenvalues are closer to the imaginary axis at a chosen stable flight condition. One may argue whether the specific physical weights chosen by Karpel are the right ones because their values depend on the value chosen for the open-loop flight condition and because the closeness of the modal eigenvalues to the imaginary axis does not necessarily indicate their relative importance. However, the attempt made by Karpel is significant since it tries to relate the accuracy of the aerodynamic Padé representation to the dynamic characteristics of the system.

In this work, it is assumed that the aerodynamic lag terms of only a small number of modes need to be represented more accurately as a function of k. These modes are the ones responsible for the open-loop flutter, with possibly some adjacent modes. These modes will be referred to as the important flutter modes. In addition, it will be assumed that equally high accuracy is required for the control surface and gust coefficients associated with the important flutter modes. Clearly these latter coefficients greatly affect the performance of the closed-loop system both in terms of stability and control surface activity. All of the other modes are considered less important, and, therefore, the aerodynamic coefficients associated with them, either directly or by coupling effects, can be allowed to tolerate larger errors. This implies that the aerodynamic terms associated directly with the important modes will be represented in a Padé form with as few lag terms as the problem permits, whereas all other aerodynamic coefficients will not be allowed any lag terms at all and they will be represented only by the quadratic expression in ik. The soundness of these assumptions cannot be measured in terms of the overall least-square error in the aerodynamic terms, but should be measured only in terms of resulting errors in the flutter parameters (like flutter dynamic pressure and flutter frequency), for both the open- and closed-loop cases. This will be described in the following sections of this work.

III. Analysis

Let the equations of motion be given by

$$[Ms^2 + K + Q_D A]\{q\} = 0 \tag{1}$$

where $[M]$, $[K]$, and $[A]$ represent the mass, stiffness, and aerodynamic matrices, respectively, and Q_D denotes the flight dynamic pressure. Equation (1) can be rewritten in the following partitioned form

$$([M_s \mid M_c]s^2 + [K_s \mid 0] + Q_D[A_s \mid A_c])\{q_s/q_c\} = -Q_D[A_G]\{q_G/V\} \tag{2}$$

where the subscripts s, c, and G relate to parameters associated with the structural modes, control surface deflections, and gust input, respectively. The matrices with the s subscripts are assumed to be of order $n_s \times n_s$, the matrices with the c subscripts are of order $n_s \times n_c$, and the matrices with the G subscripts are of order $n_s \times n_G$.

The structural related matrices will be partitioned so that different aerodynamic representation may be applied to the different partitions. Thus, Eq. (2) can be written in the following form:

$$\left(\left[\begin{array}{c|c|c} M_{s,11} & M_{s,12} & M_{c,1} \\ \hline M_{s,21} & M_{s,22} & M_{c,2} \end{array}\right]s^2 + \left[\begin{array}{c|c|c} K_{s,11} & K_{s,12} & 0 \\ \hline K_{s,21} & K_{s,22} & 0 \end{array}\right] + Q_D\left[\begin{array}{c|c|c} A_{s,11} & A_{s,12} & A_{c,1} \\ \hline A_{s,21} & A_{s,22} & A_{c,2} \end{array}\right]\right)\left\{\begin{array}{c} q_{s,1} \\ q_{s,2} \\ \hline q_c \end{array}\right\} = -Q_D\left[\begin{array}{c} A_{G,1} \\ \hline A_{G,2} \end{array}\right]\left\{\frac{q_G}{V}\right\} \tag{3}$$

It will be assumed that all the n_i important modes responsible for flutter are assembled within the partition subscripted by $s,11$. Therefore, the aerodynamic matrix $[A_{s,11}]$ will be represented in Padé form with n_L lag terms. Similarly, the control surfaces' aerodynamic coefficients $[A_{c,1}]$ and the gust force aerodynamic coefficients $[A_{G,1}]$ associated with the n_i important flutter modes will also be represented in Padé form with n_L lag terms. All other aerodynamic matrices (that is, $A_{s,12}$, $A_{s,21}$, $A_{s,22}$, $A_{c,2}$, $A_{G,2}$) will be represented by quadratic polynomials involving the reduced frequency k, using zero lag terms.

Thus, the different aerodynamic matrices will be represented as follows:

$$[A_{s,11}]=[A_{0,s,11}]+[A_{1,s,11}]\frac{b}{V}s+[A_{2,s,11}]\frac{b^2}{V^2}s^2+\sum_{j=1}^{n_L}\frac{[A_{2+j,s,11}]s}{[s+(V/b)\beta j]}$$

$$[A_{s,12}]=[A_{0,s,12}]+[A_{1,s,12}]\frac{b}{V}s+[A_{2,s,12}]\frac{b^2}{V^2}s^2$$

$$[A_{s,21}]=[A_{0,s,21}]+[A_{1,s,21}]\frac{b}{V}s+[A_{2,s,21}]\frac{b^2}{V^2}s^2$$

$$[A_{s,22}]=[A_{0,s,22}]+[A_{1,s,22}]\frac{b}{V}s+[A_{2,s,22}]\frac{b^2}{V^2}s^2$$

$$[A_{c,1}]=[A_{0,c,1}]+[A_{1,c,1}]\frac{b}{V}s+[A_{2,c,1}]\frac{b^2}{V^2}s^2+\sum_{j=1}^{n_L}\frac{[A_{2+j,c,1}]s}{[s+(V/b)\beta j]}$$

$$[A_{c,2}]=[A_{0,c,2}]+[A_{1,c,2}]\frac{b}{V}s+[A_{2,c,2}]\frac{b^2}{V^2}s^2$$

$$[A_{G,1}]=[A_{0,G,1}]+[A_{1,G,1}]\frac{b}{V}s+[A_{2,G,1}]\frac{b^2}{V^2}s^2+\sum_{j=1}^{n_L}\frac{[A_{2+j,G,1}]s}{[s+(V/b)\beta j]}$$

$$[A_{G,2}]=[A_{0,G,2}]+[A_{1,G,2}]\frac{b}{V}s+[A_{2,G,2}]\frac{b^2}{V^2}s^2 \tag{4}$$

Denote

$$\{x_{\beta j}\}=Q_D\frac{[A_{2+j,s,11}]}{[s+(V/b)\beta j]}s\{q_{s,1}\}+Q_D\frac{[A_{2+j,c,1}]}{[s+(V/b)\beta j]}s\{q_c\}+Q_D\frac{[A_{2+j,G,1}]}{[s+(V/b)\beta j]}s\begin{Bmatrix}q_G\\V\end{Bmatrix} \tag{5}$$

The vector $\{x_{\beta j}\}$ is of the same dimension as the vector $\{q_{s,1}\}$. Substituting Eqs. (4) and (5) into Eq. (3) yields

where

$$[C_{2,s,ij}]=\left[M_{s,ij}+Q_DA_{2,s,ij}\frac{b^2}{V^2}\right]$$

$$[C_{1,s,ij}]=\left[Q_DA_{1,s,ij}\frac{b}{V}\right]$$

$$[C_{0,s,ij}]=[K_{s,11}+Q_DA_{0,s,ij}]$$

$$[C_{2,c,i}]=\left[M_{c,i}+Q_DA_{2,c,i}\frac{b^2}{V^2}\right]$$

$$[C_{1,c,i}]=\left[Q_DA_{1,c,i}\frac{b}{V}\right]$$

$$[C_{0,c,i}]=[Q_DA_{0,c,i}]$$

$$[C_{2,G,i}]=\left[Q_DA_{2,G,i}\frac{b^2}{V^2}\right]$$

$$[C_{1,G,i}]=\left[Q_DA_{1,G,i}\frac{b}{V}\right]$$

$$[C_{0,G,i}]=[Q_DA_{0,G,i}]$$

$$[\bar{I}]=[I_{n_i}\ldots I_{n_i}]$$

$$\{x_\beta\}=\begin{Bmatrix}x_{\beta1}\\x_{\beta2}\\\vdots\\x_{\beta nL}\end{Bmatrix} \tag{8}$$

and where $\{x_\beta\}$ denotes the total vector of aerodynamic augmented states of dimension

$$n_a=n_i\times n_L \tag{9}$$

$$\left[\begin{array}{ccc|c}\left(M_{s,11}+Q_DA_{2,s,11}\frac{b^2}{V^2}\right)s^2+ & \left(M_{s,12}+Q_DA_{2,s,12}\frac{b^2}{V^2}\right)s^2+ & \left(M_{c,1}+Q_DA_{2,c,1}\frac{b^2}{V^2}\right)s^2+ & \\ Q_DA_{1,s,11}\frac{b}{V}s+K_{s,11}+Q_DA_{0,s,11} & Q_DA_{1,s,12}\frac{b}{V}s+K_{s,12}+Q_DA_{0,s,12} & Q_DA_{1,c,1}\frac{b}{V}s+Q_DA_{0,c,1} & I_{n_i}\ldots I_{n_i}\\ \hline \left(M_{s,21}+Q_DA_{2,s,21}\frac{b^2}{V^2}\right)s^2+ & \left(M_{s,22}+Q_DA_{2,s,22}\frac{b^2}{V^2}\right)s^2+ & \left(M_{c,2}+Q_DA_{2,c,2}\frac{b^2}{V^2}\right)s^2+ & \\ Q_DA_{1,s,21}\frac{b}{V}s+K_{s,21}+Q_DA_{0,s,21} & Q_DA_{1,s,22}\frac{b}{V}s+K_{s,22}+Q_DA_{0,s,22} & Q_DA_{1,c,2}\frac{b}{V}s+Q_DA_{0,c,2} & \end{array}\right]\begin{Bmatrix}q_{s,1}\\q_{s,2}\\q_c\\x_{\beta j}\\\vdots\\x_{\beta nL}\end{Bmatrix}$$

$$=-Q_D\left[\begin{array}{c}A_{2,G,1}\frac{b^2}{V^2}s^2+A_{1,G,1}\frac{b}{V}s+A_{0,G,1}\\ \hline A_{2,G,2}\frac{b^2}{V^2}s^2+A_{1,G,2}\frac{b}{V}s+A_{0,G,2}\end{array}\right]\begin{Bmatrix}q_G\\V\end{Bmatrix} \tag{6}$$

where I_{n_i} is a unit matrix of order n_i. Equation (6) can be written more concisely in the following form (after some rearrangement):

$$\left[\begin{array}{cc|c}C_{2,s,11}s^2+C_{1,s,11}s+C_{0,s,11} & C_{2,s,12}s^2+C_{1,s,12}s+C_{0,s,12} & \bar{I}\\ \hline C_{2,s,21}s^2+C_{1,s,21}s+C_{0,s,21} & C_{2,s,22}s^2+C_{1,s,22}s+C_{0,s,22} & 0\end{array}\right]\begin{Bmatrix}q_{s,1}\\q_{s,2}\\x_\beta\end{Bmatrix}$$

$$+\left[\begin{array}{cc|c}C_{2,c,1}s^2+C_{1,c,1}s+C_{0,c,1} & C_{2,G,1}s^2+C_{1,G,1}s+C_{0,G,1} & \\ \hline C_{2,c,2}s^2+C_{1,c,2}s+C_{0,c,2} & C_{2,G,2}s^2+C_{1,G,2}s+C_{0,G,2} & \end{array}\right]\begin{Bmatrix}q_c\\ \hline \frac{q_G}{V}\end{Bmatrix}=0 \tag{7}$$

Equation (7) can be reduced further to the form

$$[C_{2,s}s^2 + C_{1,s}s + C_{0,s} \mid I_0]\left\{\begin{array}{c} q_s \\ \hline x_\beta \end{array}\right\} + [C_{2,c}s^2 + C_{1,c}s + C_{0,c} \mid C_{2,G}s^2 + C_{1,G}s + C_{0,G}]\left\{\begin{array}{c} q_c \\ \hline \frac{q_G}{V} \end{array}\right\} = 0 \tag{10}$$

where

$$[C_{i,s}] = \left[\begin{array}{c|c} C_{i,s,11} & C_{i,s,12} \\ \hline C_{i,s,21} & C_{i,s,22} \end{array}\right]$$

$$[C_{i,c}] = \left[\begin{array}{c} C_{i,c,1} \\ \hline C_{i,c,2} \end{array}\right]$$

$$[C_{i,G}] = \left[\begin{array}{c} C_{i,G,1} \\ \hline C_{i,G,2} \end{array}\right]$$

$$\{q_s\} = \left\{\begin{array}{c} q_{s,1} \\ \hline q_{s,2} \end{array}\right\}$$

$$[I_0] = \left[\begin{array}{c} \bar{I} \\ 0 \end{array}\right] \tag{11}$$

Equation (5) can be added to the set of equations represented by Eq. (10) after bringing both sets of equations to the following form:

$$C_{2,s}s\dot{q}_s + C_{1,s}\dot{q}_s + C_{0,s}q_s + I_0 x_\beta + C_{2,c}\ddot{q}_c + C_{1,c}\dot{q}_c + C_{0,c}q_c + C_{2,G}\frac{\ddot{q}_G}{V} + C_{1,G}\frac{\dot{q}_G}{V} + C_{0,G}\frac{q_G}{V} = 0$$

$$s\{x_{\beta j}\} + \frac{V}{b}\beta_j\{x_{\beta j}\} = Q_D\left([A_{2+j,s,11}]\{\dot{q}_{s,1}\} + [A_{2+j,c,1}]\{\dot{q}_c\} + [A_{2+j,G,1}]\left\{\frac{\dot{q}_G}{V}\right\}\right) \tag{12}$$

or, in a unified matrix equation

$$s\left\{\begin{array}{c} q_s \\ \hline \dot{q}_s \\ \hline x_\beta \end{array}\right\} = \left[\begin{array}{c|c|c} 0 & I & 0 \\ \hline \bar{C}_{0,s} & \bar{C}_{1,s} & I_0 \\ \hline & B_{1,s,11}\ \ 0 & -\frac{V}{b}\beta_1 I \\ \hline & B_{2,s,11}\ \ 0 & -\frac{V}{b}\beta_2 I \\ \hline & \vdots & \ddots \\ \hline & B_{n_L,s,11}\ \ 0 & -\frac{V}{b}\beta_{n_L} I \end{array}\right] \times \left\{\begin{array}{c} q_s \\ \hline \dot{q}_{s,1} \\ \dot{q}_{s,2} \\ \hline x_{\beta 1} \\ x_{\beta 2} \\ \vdots \\ x_{\beta n_L} \end{array}\right\}$$

$$+ \left[\begin{array}{c|c|c|c|c|c} 0 & & & & & \\ \hline \bar{C}_{2,c} & \bar{C}_{1,c} & \bar{C}_{0,c} & \bar{C}_{2,G} & \bar{C}_{1,G} & \bar{C}_{0,G} \\ \hline & B_{1,c,1} & & & B_{1,G,1} & \\ \hline & B_{2,c,1} & & & B_{2,G,1} & \\ \hline & \vdots & & & \vdots & \\ \hline & B_{n_L,c,1} & & & B_{n_L,G,1} & \end{array}\right] \left\{\begin{array}{c} \ddot{q}_c \\ \hline \dot{q}_c \\ \hline q_c \\ \hline q_G/V \\ \hline \dot{q}_G/V \\ \hline q_G/V \end{array}\right\} \tag{13}$$

where

$$[\bar{C}_{l,s}] = -[C_{2,s}]^{-1}[C_{l,s}] \qquad [B_{l,s,11}] = Q_D[A_{2+l,s,11}]$$
$$[\bar{C}_{l,c}] = -[C_{2,s}]^{-1}[C_{l,c}] \qquad [B_{l,c,1}] = Q_D[A_{2+l,c,1}]$$
$$[\bar{C}_{l,G}] = -[C_{2,s}]^{-1}[C_{l,G}] \qquad [B_{l,G,1}] = Q_D[A_{2+l,G,1}]$$
$$[\bar{I}_0] = -[C_{2,s}]^{-1}[I_0] \tag{14}$$

Equation (13) can be written as

$$s\{x\} = [A_s]\{x\} + [B_c \mid B_G]\left\{\begin{array}{c} \ddot{q}_c \\ \dot{q}_c \\ q_c \\ \ddot{q}_G/V \\ \dot{q}_G/V \\ q_G/V \end{array}\right\} \tag{15}$$

where

$$\{x\} = \left\{\begin{array}{c} q_s \\ \dot{q}_s \\ x_\beta \end{array}\right\} \tag{16}$$

Equation (15) can be augmented further by adding the actuator and the gust equations, that is

$$\{\dot{x}_{ac}\} = [A_{ac}]\{x_{ac}\} + [B_{ac}]\{u\} \tag{17}$$

with the following actuator output equation

$$\left\{\begin{array}{c} \ddot{q}_c \\ \dot{q}_c \\ q_c \end{array}\right\} = [C_{ac}]\{x_{ac}\} \tag{18}$$

and for the gust

$$\{\dot{x}_G\} = [A_G]\{x_G\} + [B_G]\{w\} \tag{19}$$

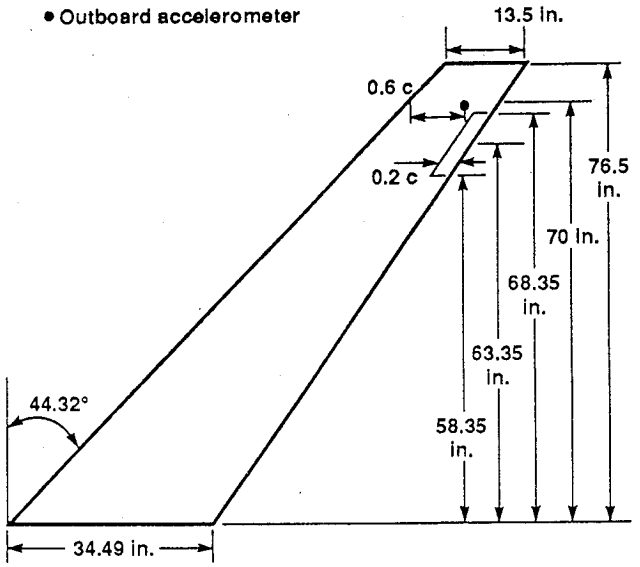

Fig. 1 Model geometry (DAST-ARW1).

with the following gust output equation

$$\begin{Bmatrix} \ddot{q}_G/V \\ \dot{q}_G/V \\ q_G/V \end{Bmatrix} = [C_G]\{x_G\} \tag{20}$$

thus yielding the following final augmented equation

$$s\begin{Bmatrix} x \\ x_{ac} \\ x_G \end{Bmatrix} = \left[\begin{array}{c|c|c} A_s & B_c C_{ac} & B_G C_G \\ \hline 0 & A_{ac} & 0 \\ \hline 0 & 0 & A_G \end{array}\right] \begin{Bmatrix} x \\ x_{ac} \\ x_G \end{Bmatrix} + \left[\begin{array}{c|c} 0 & 0 \\ \hline B_{ac} & 0 \\ \hline 0 & B_G \end{array}\right] \begin{Bmatrix} u \\ \omega \end{Bmatrix} \tag{21}$$

Equation (21) is in the canonical state-space form and it includes $n_a (= n_i \times n_L)$ augmented states due to the aerodynamic representation. These aerodynamic states are denoted in Eq. (16) by the vector $\{x_\beta\}$ [see Eqs. (8) and (5)].

It may be mentioned here that the aforementioned formulation leads, for any given number of important modes n_i and lag terms n_L, to a minimum number of augmented states. The basic idea in this paper could have also been implemented using the column dependent modified matrix Padé method[6] with a single lag term allowed in the columns associated with the important flutter modes, control surface modes, and gust input mode, with no lag terms allowed in all other columns. However, this would have resulted in a large number n_a of aerodynamic augmented states.

IV. Results

A. Description of the Mathematical Models

The method proposed in this work will be applied to two mathematical models, NASA's Drone for Aerodynamic and Structural Testing, Aerodynamic Research Wing 1 (DAST-ARW1), and the YF-17 fighter model.

The DAST-ARW1 mathematical model[10] consists of 10 elastic symmetric modes and one trailing-edge (TE) control surface (see Fig. 1). The aerodynamic coefficients for this case were computed using NASA's interaction structures aerodynamics controls (ISAC) program (which employs doublet lattice aerodynamics) at Mach number $M = 0.9$. The proposed method will be tested using the open-loop case and also two closed-loop cases. The closed-loop cases will be based on two different control laws. The first control law, which will be referred to as control law 1 (CL 1), was developed in Ref. 9 and is given by

$$\frac{\delta_c}{\ddot{h}_{outb}} = \frac{2214}{(s+10)}\frac{s}{(s+1)}\left[\frac{s^2+30.79s+14{,}692}{s^2+572.6s+88{,}578}\right] \times \left[\frac{s^2+47.37s+72{,}436}{s^2+568.6s+86{,}972}\right]\frac{\text{deg}}{g} \tag{22}$$

The second control law, which will be referred to as control law 2 (CL 2), was developed using the aerodynamic energy

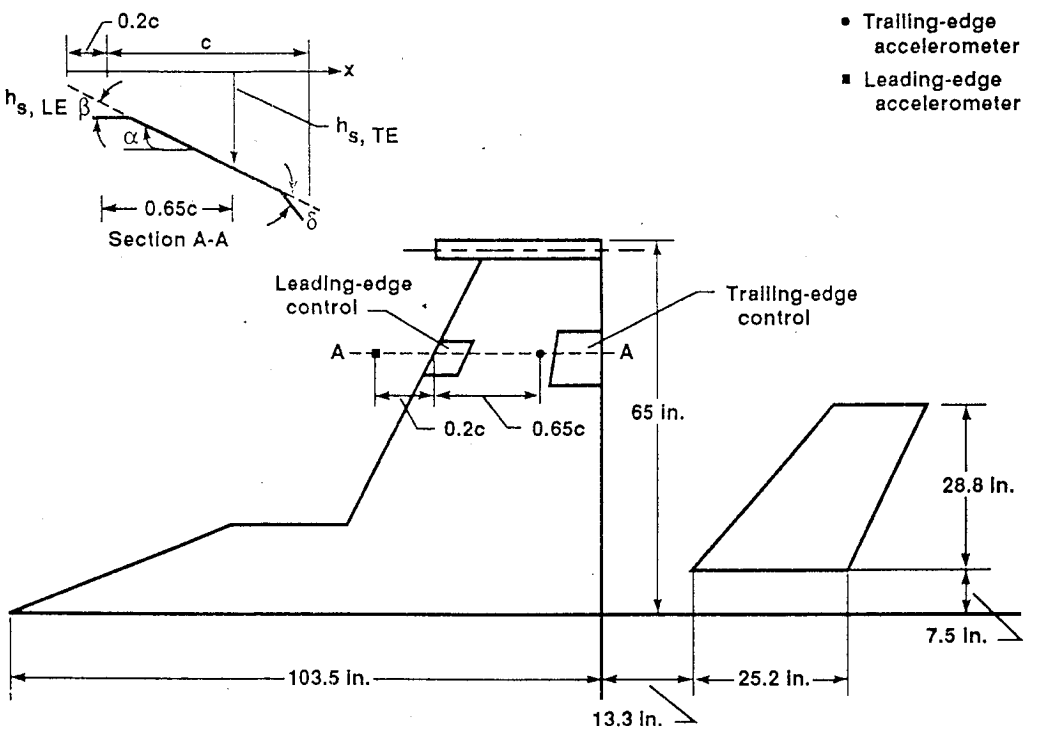

Fig. 2 Plan view of YF-17 flutter model.

Table 1 Summary of flutter results associated with the DAST-ARW1 mathematical model, using Padé representation of the full aerodynamic matrix, together with the results of the proposed method

Case description	n_a	Q_F, lb/ft^2	ω_F, rad/s	Percentage errors $\Delta Q_F/Q_F$, %	Percentage errors $\Delta\omega_F/\omega_F$, %
Open loop					
4 lag terms[a]	40	99.9	50.2	0.0	0.0
3 lag terms	30	98.4	49.9	−1.5	−0.6
2 lag terms	20	99.6	50.1	−0.3	−0.2
1 lag term	10	100.1	50.1	0.2	−0.2
0 lag terms	0	115.6	62.3	15.7	24.1
Proposed method	2	100.0	50.1	0.1	−0.2
Closed loop using control law 1					
4 lag terms[a]	40	174.3	48.8	0.0	0.0
3 lag terms	30	171.3	50.0	−1.7	2.4
2 lag terms	20	172.5	48.7	−1.0	−0.2
1 lag term	10	178.9	49.1	2.6	0.6
0 lag terms	0	141.8	59.3	−18.6	21.5
Proposed method	2	167.5	51.3	−3.9	5.1
Closed loop using control law 2					
4 lag terms[a]	40	206.4	29.5	0.0	0.0
3 lag terms	30	207.9	29.7	0.7	0.7
2 lag terms	20	204.3	30.3	−1.0	2.7
1 lag term	10	209.6	28.4	1.6	−3.7
0 lag terms	0	177.8	49.2	−13.9	66.8
Proposed method	2	207.8	30.6	0.7	3.7

[a]Results considered exact.

approach (in a work that is currently being processed for publication by NASA) and is given by

$$\frac{\delta_c}{\ddot{h}_{\text{outb}}/\text{b}} = 4.39 \times 10^{-4} \frac{s+185.8}{s+630} \times \frac{s^2+155s+29{,}658}{s^2+13.53s+272.25} \text{ rad} \tag{23}$$

where $b = 7.6416$ in. and δ_c is the actuator command signal. The actuator transfer function for the above two control laws is given by

$$\frac{\delta}{\delta_c} = \frac{1.915 \times 10^7}{(s+214)(s^2+179.4s+89{,}450)} \frac{\text{deg}}{\text{deg}} \tag{24}$$

where δ is the TE control deflection, positive TE down.

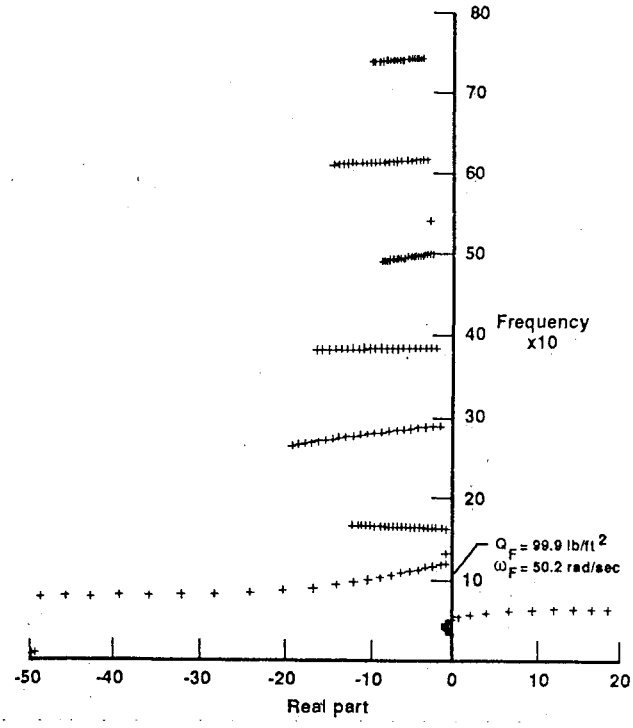

Fig. 3 Open-loop root-locus plot—DAST-ARW1 mathematical model. Aerodynamic representation using four lag terms, resulting in 40 augmented states ($n_i = 10$).

The YF-17 mathematical model[11] consists of two rigid-body modes and 10 elastic modes and has both a leading-edge (LE) and a TE control surface, as shown in Fig. 2. Here, again, the proposed method will be tested using the open-loop and closed-loop cases where both control surfaces are simultaneously activated using the following control laws (based on unpublished work using a combination of aerodynamic and inertial energy methods):

For the TE control

$$\delta = \frac{-3343.3}{(s^2+17.76s+1971.4)(s^2+2s+1)} \frac{\ddot{h}_{s,\text{TE}}}{b} \text{ rad} \tag{25}$$

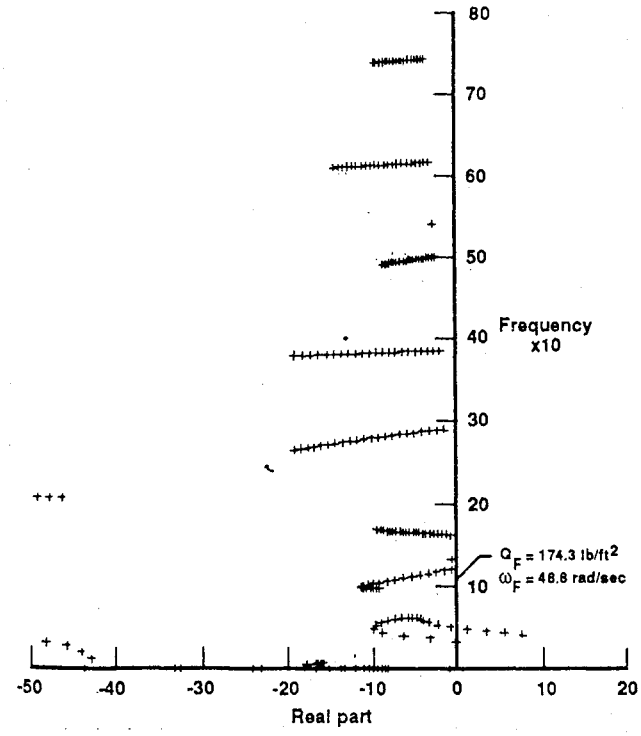

Fig. 4 Closed-loop root-locus plot—DAST-ARW1 mathematical model with one active control surface, using control law 1. Aerodynamic representation using four lag terms, resulting in 40 augmented states ($n_i = 10$).

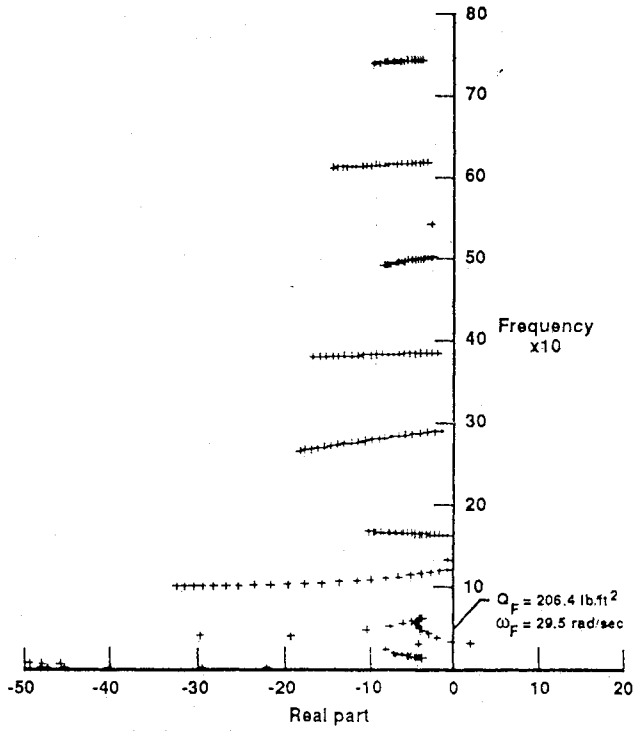

Fig. 5 Closed-loop root-locus plot—DAST-ARW1 mathematical model with one active control surface, using control law 2. Aerodynamic representation using four lag terms, resulting in 40 augmented states ($n_i = 10$).

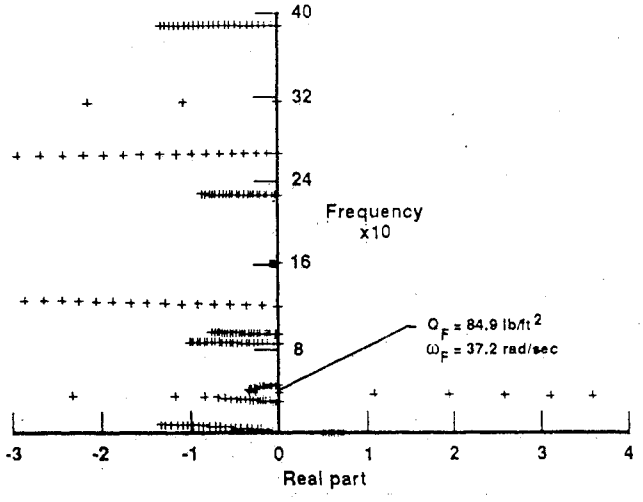

Fig. 6 Open-loop root-locus plot—YF-17 mathematical model. Aerodynamic representation using four lag terms and $n_i = 12$, resulting in 48 augmented states.

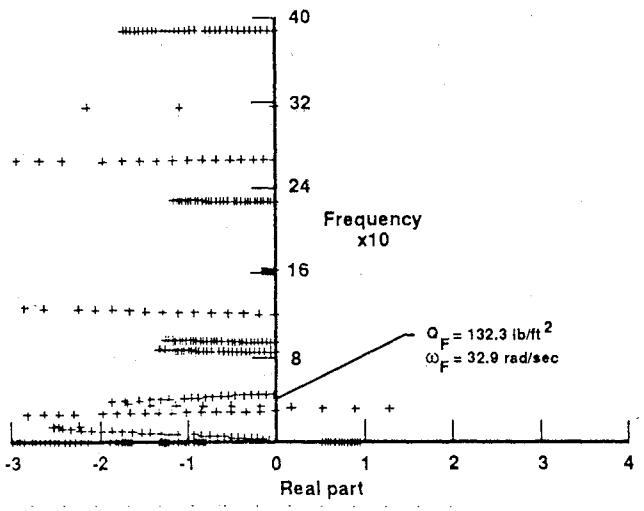

Fig. 7 Closed-loop root-locus plot—YF-17 mathematical model, using two active control surfaces. Aerodynamic representation using four lag terms and $n_i = 12$, resulting in 48 augmented states.

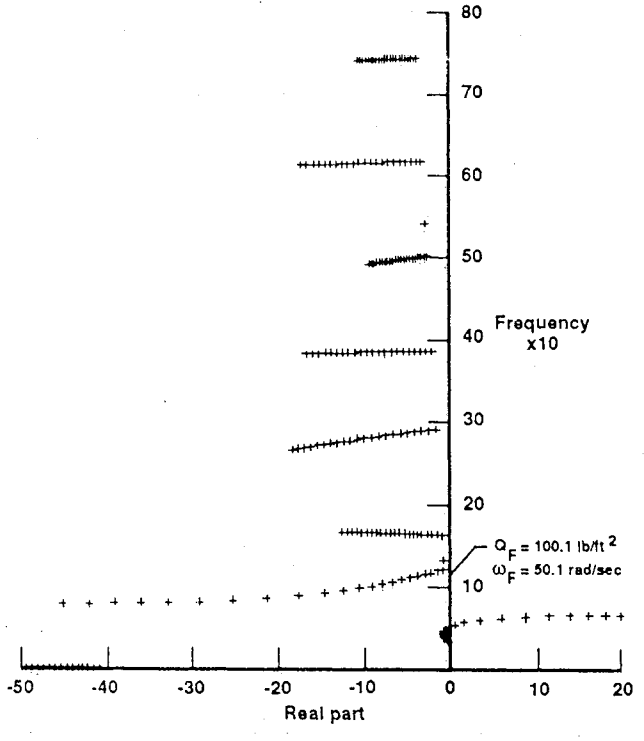

Fig. 8 Open-loop root-locus plot—DAST-ARW1 mathematical model. Aerodynamic representation using one lag term, resulting in 10 augmented states ($n_i = 10$).

and for the LE control

$$\beta = \frac{4740.5}{(s^2 + 15.65s + 1531.2)(s^2 + 4s + 4)} \frac{\ddot{h}_{s,\mathrm{LE}}}{b} \text{ rad} \qquad (26)$$

where β is the deflection of the LE control (positive nose down), and $\ddot{h}_{s,\mathrm{TE}}$ and $\ddot{h}_{s,\mathrm{LE}}$ denote the accelerometer readings located along the TE control midspan section at the 65 and -20% chord locations, respectively (see Fig. 2). The -20% chord location can in practice be achieved by using two accelerometers, which, when extrapolated, yield the -20% chord value for $\ddot{h}_{s,\mathrm{LE}}$. Here again, b is the semichord length at the accelerometer's wing-span section and has the value of $b = 12.4894$. In the YF-17 case, no actuator dynamics are modeled, and the aerodynamics are evaluated at $M = 0.9$ using doublet lattice program.

B. Presentation and Discussion of Results

The first stage in the present work was to determine the effect of the number of lag terms on the flutter parameters, that is, on the flutter dynamic pressure Q_F and the flutter frequency ω_F. In this initial stage, *all* of the modes are considered equally important, and both open- and closed-loop cases are tested. Table 1 summarizes the results for the DAST-ARW1 case and Table 2 summarizes the results for the YF-17 case. In both cases, the results associated with the four lag terms are considered to be the most accurate and will be referred to, herein, as the exact results. The lag terms used for the DAST-ARW1 case are $\beta_1 = 0.1$, $\beta_2 = 0.2$, $\beta_3 = 0.3$, and $\beta_4 = 0.4$. In the case of a single lag term, only β_1 is used. For the case of two lag terms, β_1 and β_2 are used, and for the case

Table 2 Summary of flutter results associated with the YF-17 mathematical model, using Padé representation of the full aerodynamic matrix, together with the results of the proposed method

Case description	n_a	Q_F, lb/ft^2	ω_F, rad/s	Percentage errors	
				$\Delta Q_F/Q_F$, %	$\Delta\omega_F/\omega_F$, %
Open loop					
4 lag terms[a]	48	84.9	37.2	0.0	0.0
3 lag terms	36	85.0	37.2	0.1	0.0
2 lag terms	24	85.0	37.2	0.1	0.0
1 lag term	12	85.9	37.3	1.2	0.3
0 lag terms	0	77.9	38.6	−8.2	3.8
Proposed method	2	85.0	37.4	0.1	0.5
Closed loop with two active control surfaces					
4 lag terms[a]	48	132.3	32.9	0.0	0.0
3 lag terms	36	132.4	32.9	0.1	0.0
2 lag terms	24	132.8	32.9	0.4	0.0
1 lag term	12	130.9	33.1	−1.1	0.6
0 lag terms	0	134.0	32.6	1.3	−0.9
Proposed method	2	128.8	33.2	−2.6	0.9

[a]Results considered exact.

Table 3 Variation of flutter results with values of the single lag term ($n_L = 1$) for DAST-ARW1 model, using Padé representation of the full aerodynamic matrix

Case description	β_1	Q_F, lb/ft^2	ω_F, rad/s	Percentage errors	
				$\Delta Q_F/Q_F$, %	$\Delta\omega_F/\omega_F$, %
Open loop	0.05	120.6	54.8	20.7	9.2
	0.10	100.1	50.1	0.2	−0.2
	0.15	97.0	49.9	−2.9	−0.6
	0.20	98.0	50.7	−1.9	1.0
	0.30	101.2	52.4	1.3	4.4
	0.40	103.4	53.5	3.5	6.6
Closed loop	0.05	181.2	50.7	4.0	3.9
using control law 1	0.10	178.9	49.1	2.6	0.6
	0.15	172.5	50.0	−1.0	2.5
	0.20	167.4	51.1	−4.0	4.7
	0.30	161.0	52.9	−7.6	8.4
	0.40	157.2	54.1	−9.8	10.9
Closed loop	0.05	217.6	27.6	5.4	−6.4
using control law 2	0.10	209.6	28.4	1.6	−3.7
	0.15	207.1	29.6	0.3	0.3
	0.20	205.4	31.1	−0.5	5.4
	0.30	202.7	33.2	−1.8	12.5
	0.40	200.8	34.5	−2.7	16.9

Table 4 Variation of flutter results with values of the single lag term ($n_L = 1$) for YF-17 model, using Padé representation of the full aerodynamic matrix

Case description	β_1	Q_F, lb/ft^2	ω_F, rad/s	Percentage errors	
				$\Delta Q_F/Q_F$, %	$\Delta\omega_F/\omega_F$, %
Open loop	0.025	85.1	37.7	0.2	1.3
	0.050	85.9	37.3	1.2	0.3
	0.075	85.9	37.2	1.2	0.0
	0.100	85.8	37.2	1.1	0.0
	0.150	85.5	37.2	0.7	0.0
	0.200	85.2	37.2	0.4	0.0
	0.250	85.0	37.2	0.1	0.0
Closed loop with two	0.025	130.4	33.0	−1.4	0.3
active control surfaces	0.050	130.9	33.1	−1.1	0.6
	0.075	131.3	33.0	−0.8	0.3
	0.100	131.7	33.0	−0.5	0.3
	0.150	132.1	32.9	−0.2	0.0
	0.200	132.3	32.9	0.0	0.0
	0.250	132.4	32.9	0.1	0.0

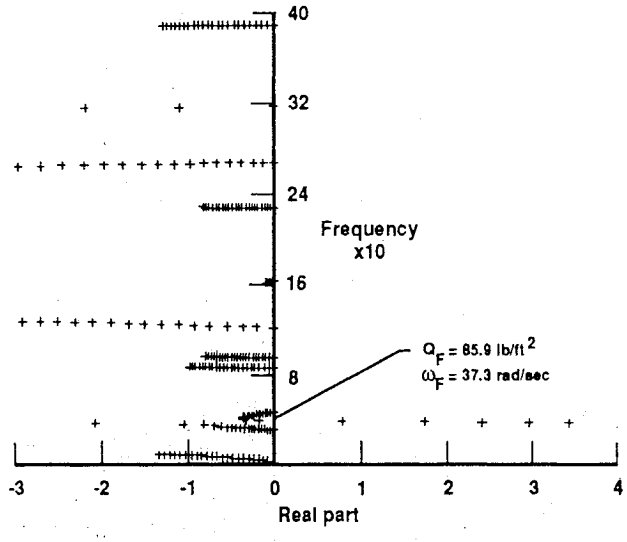

Fig. 9 Open-loop root-locus plot—YF-17 mathematical model. Aerodynamic representation using one lag term resulting in 10 augmented states ($n_i = 10$).

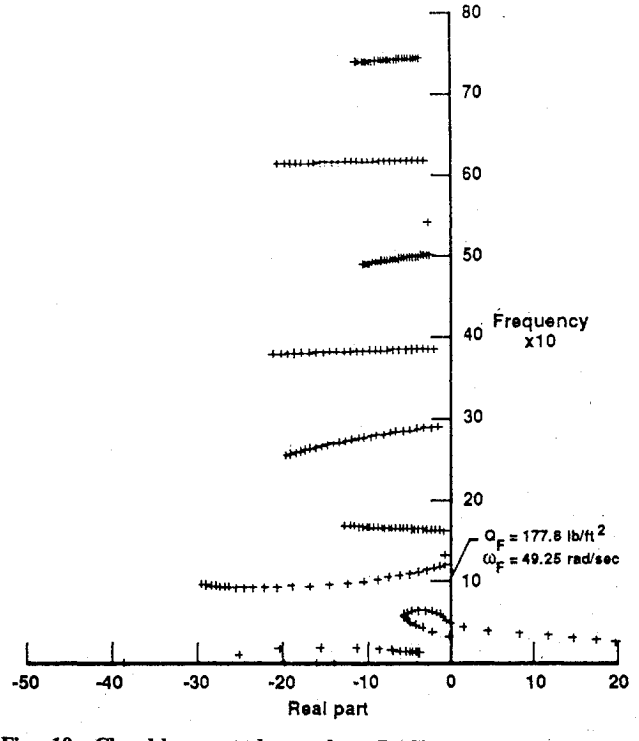

Fig. 10 Closed-loop root-locus plot—DAST-ARW1 mathematical model with one active control surface, using control law 2. Aerodynamic representation using zero lag terms resulting in no augmented states.

of 3 lag terms, β_1, β_2, and β_3 are used. Similarly, for the YF-17 case, the lag terms used are given by

$$\beta_1 = 0.05, \quad \beta_2 = 0.2, \quad \beta_3 = 0.3, \quad \beta_4 = 0.4$$

For the case denoted as zero lag terms, only the quadratic part of the Padé representation was used.

The root-locus plots associated with the four lag terms (the exact results) will form the reference for comparison against all other results. Figures 3–5 present the root-locus plots associated with the DAST-ARW1 case, and Figs. 6 and 7 show similar results for the YF-17 case. As can be seen from Tables 1 and 2, a single lag term yields very good accuracy regarding the flutter parameters, with errors of less than 3.7% in *all cases*. As examples, the root-locus plots associated with the open-loop case are presented in Fig. 8 for the DAST-ARW1 case and in Fig. 9 for the YF-17 case. Comparisons between these root-locus plots (Figs. 8 and 9) and their counterparts associated with the four lag terms (Figs. 3–7) show that the general behavior is identical and that any differences are very small. However, when zero lag terms are assumed, large errors can be observed, especially in the DAST-ARW1 case, reaching values as high as 66.8%. Furthermore, even for the DAST-ARW1 open-loop case, where the errors in Q_F and ω_F are only 15.7 and 24.1%, respectively, the root-locus plot (not shown here) shows a significant difference compared to the four lag terms case

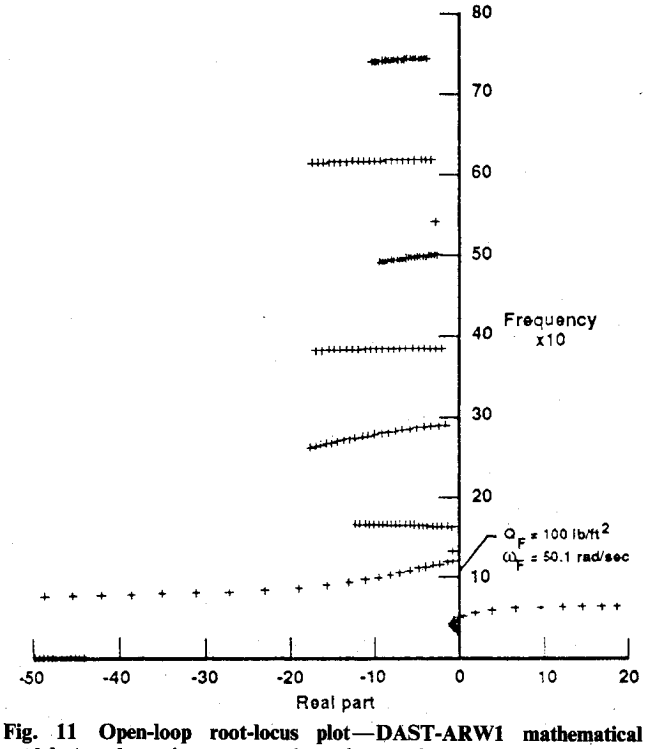

Fig. 11 Open-loop root-locus plot—DAST-ARW1 mathematical model. Aerodynamic representation using one lag term resulting in two augmented states ($n_i = 2$).

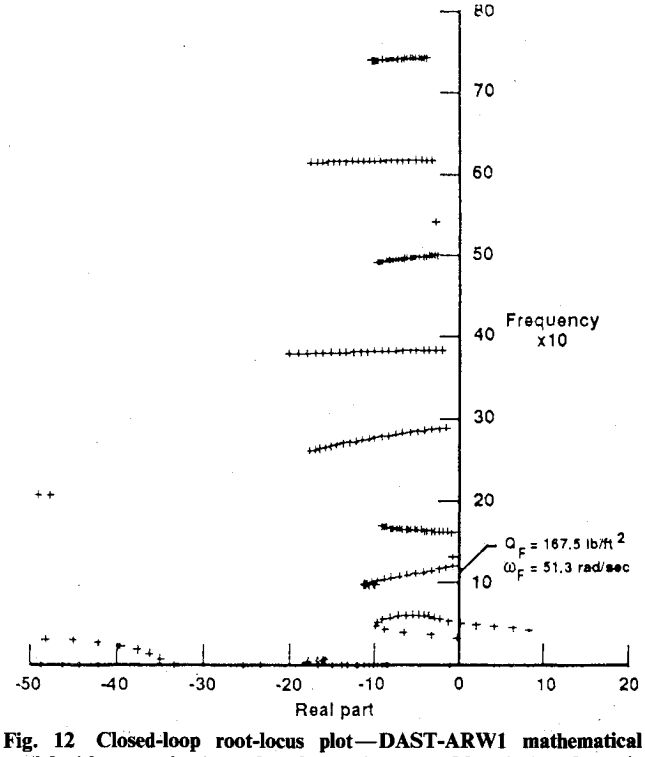

Fig. 12 Closed-loop root-locus plot—DAST-ARW1 mathematical model with one active control surface, using control law 1. Aerodynamic representation using one lag term resulting in two augmented states ($n_i = 2$).

Table 5 Variation of flutter results with number of augmented states, using Padé representation of selected modes only; closed loop using control law 1, DAST-ARW1

Modes represented in Padé form	n_a	Q_F, lb/ft^2	ω_F, rad/s	Percentage errors	
				$\Delta Q_F/Q_F$, %	$\Delta\omega_F/\omega_F$, %
$n_L = 1$					
1,2	2	167.5	51.3	−3.9	5.1
1,2,3	3	167.5	51.3	−3.9	5.1
1,2,4	3	170.6	51.1	−2.1	4.7
1,2,4,5	4	180.7	48.6	3.7	−0.4
1,2,4,5,6	5	179.0	49.0	2.7	0.4
1,2,4,5,6,7	6	178.6	49.1	2.5	0.6
1,2,4,5,6,7,8,9,10	9	178.9	49.1	2.6	0.6
$n_L = 2$					
1,2	4	164.0	51.3	−5.9	5.1
1,2,3	6	164.0	51.3	−5.9	5.1
1,2,4	6	166.4	50.7	−4.5	3.9
1,2,4,5	8	173.7	48.3	−0.3	−1.0
1,2,4,5,6	10	172.6	48.7	−1.0	−0.2
1,2,4,5,6,7	12	172.4	48.7	−1.1	−0.2
1,2,4,5,6,7,8,9,10	18	172.5	48.7	−1.0	−0.2
$n_L = 3$					
1,2	6	162.2	52.0	−6.9	6.6
1,2,3	9	162.2	52.0	−6.9	6.6
1,2,4	9	164.5	51.8	−5.6	6.1
1,2,4,5	12	172.5	49.5	−1.0	1.4
1,2,4,5,6	15	171.4	49.9	−1.7	2.3
1,2,4,5,6,7	18	171.2	50.0	−1.8	2.5
1,2,4,5,6,7,8,9,10	27	171.3	50.0	−1.7	2.5
$n_L = 4$					
1,2	8	164.1	51.4	−5.9	5.3
1,2,3	12	164.1	51.4	−5.9	5.3
1,2,4	12	167.4	50.9	−4.0	4.3
1,2,4,5	16	175.3	48.5	0.6	−0.6
1,2,4,5,6	20	174.4	48.8	0.1	0.0
1,2,4,5,6,7	24	174.2	48.9	−0.1	0.2
1,2,4,5,6,7,8,9,10	36	174.3	48.8	0.0	0.0

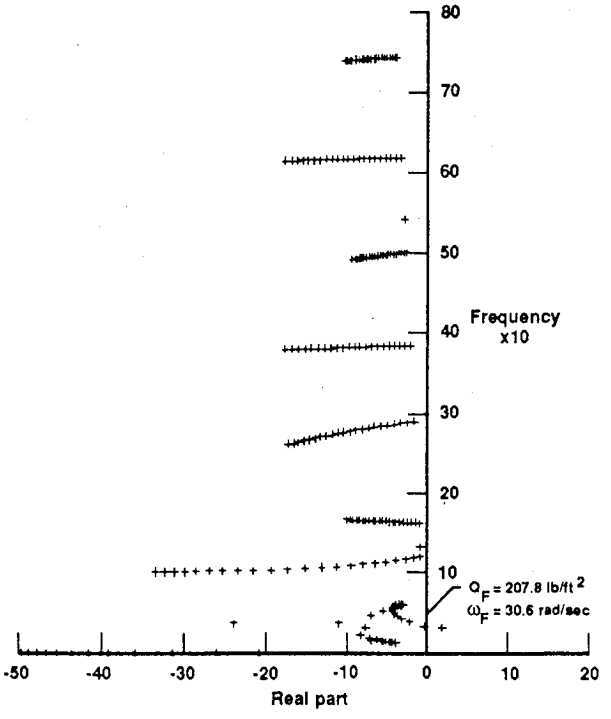

Fig. 13 Closed-loop root-locus plot—DAST-ARW1 mathematical model with one active control surface, using control law 2. Aerodynamic representation using one lag term resulting in two augmented states ($n_i = 2$).

(Fig. 3). The largest errors are observed for the DAST-ARW1 closed-loop case, using CL 2. The root-locus plot for this case, using zero lag terms, is shown in Fig. 10. As can be seen, Fig. 10 shows significant differences when compared with Fig. 5, which relates to the same case but with four lag terms.

At this stage it can be concluded that a single lag term can successfully maintain all the required dynamic characteristics of the fluttering system, even when the closed-loop systems show large increases in Q_F and also large changes in ω_F. However, it was thought that the numerical values chosen for the single lag term approximation need to be investigated. The values for β_1 were chosen in this work to be around the open-loop values associated with the flutter reduced frequency k_F. The DAST-ARW1 open-loop flutter is at $k_F = 0.093$ and the YF-17 open-loop flutter is at $k_F = 0.042$. This is the reason β_1 was assigned the values of $\beta_1 = 0.1$ and 0.05 for the two examples used here.

The effects of varying β_1 in a single lag Padé representation involving *all* of the modes is summarized in Table 3 for the DAST-ARW1 example and in Table 4 for the YF-17 example. As can be seen, the smallest errors in the flutter parameters are obtained when β_1 is assigned a value around the open-loop value of k_F, with slightly higher values preferred over lower ones. It is interesting to note that when β_1 is smaller than the open-loop value of k_F, the DAST-ARW1 example shows relatively large errors, especially for the open-loop case, where the errors reach levels of 20.7% in Q_F and 9.2% in ω_F. The value of β_1 needs to be significantly larger than the open-loop value of k_F to show relatively large errors. Table 3 for the DAST-ARW1 example shows errors of 10.9 and 16.9% in the flutter parameters when $\beta_1 = 0.4$ (in the closed-loop cases).

In all of the results presented so far, the YF-17 example showed much less sensitivity to both the number of lag terms

and the assigned values for β_1. A possible reason for this insensitivity can be attributed to the different flutter mechanisms. The YF-17 example relates to an external store type of flutter of a relatively stiff wing, whereas the DAST-ARW1 relates to a classical wing bending-torsion flutter of a relatively flexible wing. Hence, the two flutter mechanisms are considerably different.

The results presented so far involved the same aerodynamic representation for *all* of the modes, using the errors in the flutter parameters as a criterion for the determination of both the number of lag terms and the value of the β_1 lag term. This is in contrast to some other works whereby the different parameters are determined by the overall residual least-square error between the tabulated and the approximated aerodynamics. In the present work, a varying number of modes was assumed to form the proposed group of the important flutter modes, and the effects of the number of important flutter modes and the number of the lag terms used to represent the aerodynamics of these modes was investigated. As may be recalled, the aerodynamics of all of the other modes is represented by a quadratic expression in *ik* with zero lag terms. An example of the results of this investigation is presented in Table 5, which relates to the closed-loop DAST-ARW1 case using CL 1. In all cases, very good results were obtained when only the first two elastic modes were assumed to form the group of important flutter modes. These latter results are presented in Tables 1 and 2.

In making the comparisons with the present method, one should remember that the exact problem, with a four lag term aerodynamic representation, gives rise to 40 augmented aerodynamic states. The results in Tables 1 and 2 relating to the proposed method give rise to only two augmented aerodynamic states. It is, therefore, very interesting to note the small errors associated with the proposed method. For the DAST-ARW1 open-loop case, errors of only 0.1% in Q_F and -0.2% in ω_F can be observed. For the closed-loop case using CL 1, errors of only 3.9% in Q_F and 5.1% in ω_F are obtained. Control law 2 yields even smaller errors (0.7% in Q_F and 3.7% in ω_F) in the flutter parameters with only two augmented aerodynamic states (Table 1).

The results relating to the YF-17 example (Table 2) yield errors that are generally lower than in the DAST-ARW1 case. For the YF-17 open-loop case, with $n_i = 2$ and $n_L = 1$, errors as low as 0.1% for Q_F and 0.5% in ω_F are obtained (Table 2). For the closed-loop case, the errors for this same case are -2.6% in Q_F and 0.9% in ω_F (Table 2). Once again, two augmented aerodynamic states appear to be sufficient.

The root-locus plots for both the DAST-ARW1 and the YF-17 examples are shown in Figs. 11–15, with aerodynamic

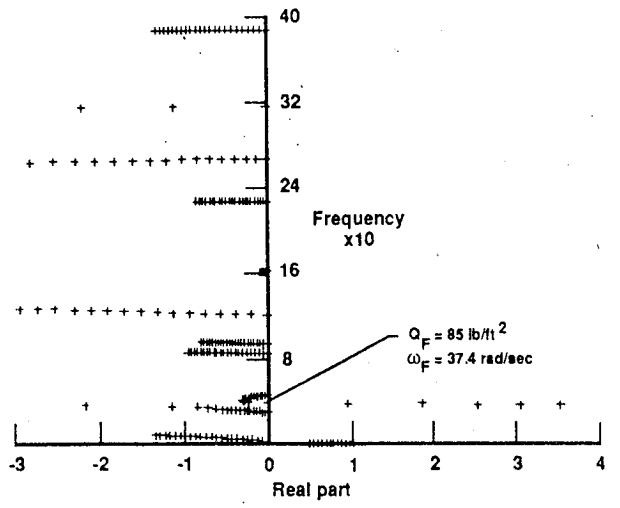

Fig. 14 Open-loop root-locus plot—YF-17 mathematical model. Aerodynamic representation using one lag term resulting in two augmented states ($n_i = 2$).

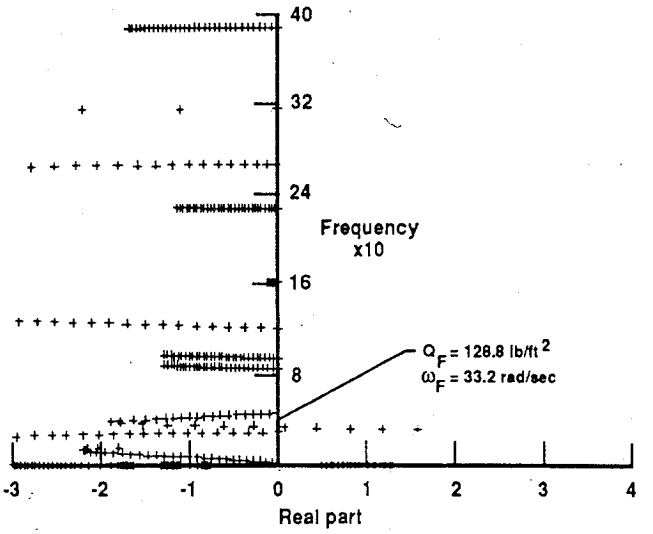

Fig. 15 Closed-loop root-locus plot—YF-17 mathematical model with two active control surfaces. Aerodynamic representation using one lag term resulting in two augmented states ($n_i = 2$).

representation yielding two augmented aerodynamic states (using $n_i = 2$ and $n_L = 1$). Figures 11–13 relate to the DAST-ARW1 case, with Fig. 11 representing the open-loop case, Fig. 12 representing the closed-loop case using CL 1, and Fig. 13 representing the closed-loop case using CL 2. In all cases, these figures are very similar to those shown in Figs. 3–5 for the case where $n_i = 10$ and $n_L = 4$ (with resulting 40 augmented aerodynamic states). Similar comparisons between Figs. 14 and 15, which relate to the YF-17 open- and closed-loop cases, respectively, and Figs. 6 and 7, which relate to the exact cases, show only negligible differences.

It should be mentioned that, in the YF-17 example, the first two modes that relate to the rigid-body modes have very little effect on the flutter parameters. For this reason, the two important flutter modes relate to modes 3 and 4, which represent the first two elastic modes.

V. Concluding Remarks

It is remarkable that in all of the cases treated in this work, a very good dynamic representation of the fluttering system could be maintained with only two augmented aerodynamic states. These results were obtained by first defining the important flutter modes, which normally is a fairly easy task, based on the open-loop root-locus plot. The aerodynamics of only these modes were represented, together with their associated control surface and gust coefficients, in a Padé form using a single lag term only. The best value for this single lag term β_1 is shown to be around k_F. Also, the flutter parameters show a significant sensitivity to values of β_1 when these latter values are smaller than k_F. Hence, one should ensure that β_1 is never smaller than either the open- or closed-loop values of k_F.

The proposed method should prove useful to the design of lower-order control laws using optimal control theory. Once the control law is formulated, one may use a more accurate aerodynamic representation to obtain more accurate results relating to the performance of the closed-loop system, should this be desired.

References

[1]Newsom, J. R., "A Method for Obtaining Practical Flutter Suppression Control Laws Using Results of Optimal Control Theory," NASA TP-1471, 1979.

[2]Gangsaas, D., and Ly, U. L., "Application of a Modified Linear Quadratic Gaussian Design to Active Control of a Transport Airplane," AIAA Paper 79-1746, Aug. 1979.

[3]Mahesh, J. K., Garrard, W. L., Stone, C. R., and Hausman, P. D., "Active Flutter Control for Flexible Vehicles," Vol. 1, NASA CR-159160, 1979.

[4]Mukhopadhyay, V., Newsom, J. R., and Abel, I., "A Method for Obtaining Reduced-Order Control Laws for High-Order Systems Using Optimization Techniques," NASA TP-1876, 1981.
[5]Roger, K. L., "Airplane Math Modeling Methods for Active Control Design," AGARD CP-228, Aug. 1977.
[6]Dunn, H. J., "An Analytical Technique for Approximating Unsteady Aerodynamics in the Time Domain," NASA TP-1738, 1980.
[7]Tiffany, S. H., and Adams, W. M., "Non-Linear Programming Extensions to Rational Function Approximation Methods for Unsteady Aerodynamic Forces," NASA TP-2776, 1988.
[8]Karpel, M., "Design for Active and Passive Flutter Suppression and Gust Alleviation," NASA CR-3482, 1981.
[9]Karpel, M., "Time-Domain Aeroservoelastic Modeling Using Weighted Unsteady Aerodynamic Forces," *Journal of Guidance, Control and Dynamics*, Vol. 13, No. 1, 1990.
[10]Newsom, J. R., Abel, I., and Dunn, H. J., "Application of Two Design Methods for Active Flutter Suppression and Wind-Tunnel Test Results," NASA TP-1653, 1980.
[11]Hwang, C., Winter, B., and Mills, G., "Demonstration of Active Wing/Store Flutter Suppression Systems," AFFDL-TR-78-65, 1978.